High frequency modeling of a quasi-optical characterization bench

Gregory Gaudin, Alain Peden, Clément Henry, Daniel Bourreau

HIGH FREQUENCY MODELING OF A QUASI-OPTICAL CHARACTERIZATION BENCH

Gregory Gaudin [1, a], Alain Peden [1], Clément Henry [1], Daniel Bourreau [1]

[1] Lab-STICC, UMR 6285 CNRS, IMT Atlantique, Technopôle Brest-Iroise, CS 83818, 29238 Brest Cedex 3, France

[a] Email: gregory.gaudin@imt-atlantique.fr

***Abstract*—This paper focuses on modelling quasi-optical elements, such as highly directive Gaussian optic lens antennas (GOLA) and dielectric slabs, using vectorial Gaussian beam expansion and tracking techniques. GOLAs are key components for free-space characterisation benches and are used in THz imaging, sensing and communication applications. The developed modelling tool is employed to model a free-space characterisation bench, which includes a dielectric slab of rexolite positioned between two GOLAs. A Thru-Reflect-Line (TRL) calibration is applied on the simulated datasets to compare the resulting S-parameters with measurements and with an analytical model of a dielectric slab.**

I. Introduction

Quasi-optical techniques for characterising materials in free space are very attractive because broadband permittivity extraction can be achieved particularly at high frequencies such as in the W, D or J band [1, 2, 3, 4, 5]. A typical free space characterisation bench consists of focusing antennas placed on either side of the material to be tested. They are carefully aligned to ensure that their optical axes coincide, guaranteeing optimal illumination for both the lenses and the material under test. This setup enables the characterisation of solid materials without any specific machining of the sample under test, as would be necessary with rectangular or coaxial waveguide cells or cavities. Current characterisations are carried out on the assumption that the material under test is large enough to intercept the incident beam. Such beam is considered as paraxial, producing a planar wavefront at the sample surface [6]. To assess the potential impact of any misplacement of quasi-optical components, one option is to electromagnetically model the quasi-optical (QO) components of the bench (e.g. horns, lenses, mirrors). Commercial software using full wave techniques are not suitable for this specific environment due to the large size of the electrical components at these frequencies, resulting in prohibitively long simulation times in the design of the test bench. To circumvent these limitations, a specifically designed modelling tool, as presented in [7], is used to simulate the test bench and to assess the effect of potential misalignments on the measured S-parameters.

The characterisation bench will be first presented. Then, the modelling tool used for simulating the bench will be introduced and subsequently applied in the modelling tool of an ideal setup for the characterisation bench. To enable comparison with both measured data and the analytical model of a dielectric slab, it will be also shown how to apply a Thru-Reflect-Line (TRL) calibration procedure on the simulated dataset.

Finally, a realistic setup is simulated, with tilt and misplacement applied on both the lenses and sample. The aim of this simulation is to investigate the effect of the bench impairments on the permittivity extraction of the slab.

II. Presentation of the characterisation bench

The antennas of the characterisation benches developed at IMT Atlantique Microwave department are Gaussian beam focusing horns, also known as *Gaussian Optic Lens Antenna* (GOLA). As illustrated in Fig. 1, the material to be characterised (MUT - Material Under Test) is placed between the antennas. The sample is held in position by non-conductive supports to avoid parasitic reflections and diffractions. Reflections can be minimised, for example by using absorbers placed around the reflecting elements to attenuate reflected waves. Moreover, the bench is designed such that most of the beam power interacts only with the MUT. A vector network analyser (VNA) is used to measure the S-parameters, which are essential for extracting material properties.

Before starting measurements, the setup is calibrated using a free-space TRL method such as the one described in [6, 8]. This helps to correct for the effects of the antennas and the VNA. The measured data is then processed to determine the electromagnetic properties of the material such as its permittivity which is extracted by comparing the measured S-parameters with the analytical model of the slab, assuming a plane wave incidence [6]. This condition is locally satisfied if the sample is placed in the waist of a Gaussian beam.

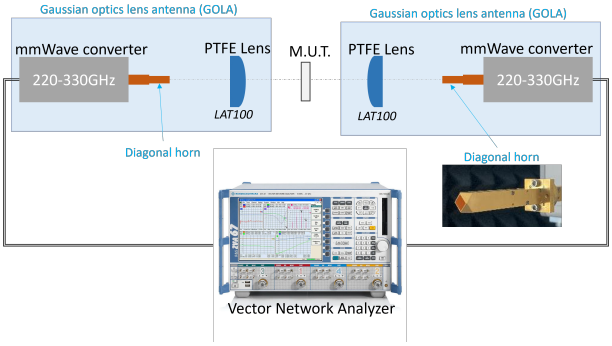

Fig. 1: Measurement setup for characterising the permittivity of the MUT

III. Modelling Tool

A. Gaussian beam expansion and tracking

Gaussian beams are commonly used for simulating quasi-optical systems [9]. The incident field is modelled with a single Gaussian beam and a ray transfer matrix analysis is performed to compute the reflected and transmitted beams. The same principle can be used to model an arbitrary electric field incoming on an expansion surface, by expanding it into elementary Gaussian beams, which reproduce the incident field propagation once combined as follows [10, 11, 9]:

$$ {}^{g}\boldsymbol{E}_i(\boldsymbol{r}_p) = \sum_{n=1}^{N} {}^{g}\mathbf{K}_n \, {}^{n}\boldsymbol{E}_{gb,n}({}^{n}\boldsymbol{r}_p), \quad \forall p \in [1, N], \quad (1) $$

where ${}^{g}E_i(\boldsymbol{r}_p)$ is the incoming field evaluated at the sampling point r_p and written in the global reference frame (g), and

$$ {}^{n}\boldsymbol{E}_{gb}({}^{n}\boldsymbol{\rho}, z) = \begin{bmatrix} \boldsymbol{\alpha} \\ -\frac{1}{2}\boldsymbol{\alpha}^T \left(\mathbf{Q}(z) + \mathbf{Q}^{\mathrm{T}}(z)\right) \boldsymbol{\rho} \end{bmatrix} u(\boldsymbol{\rho}, z), \quad (2) $$

the nth elementary Gaussian beam written in its local frame (n), ${}^{n}\boldsymbol{\rho}$ the transverse coordinates written in frame (n), $\mathbf{Q} \in \mathbf{C}^{2\times 2}$ the complex curvature matrix and $\boldsymbol{\alpha} \in \mathbf{C}^2$ a couple of transverse polarisation coefficients. The longitudinal component is derived from the partial derivatives of the transverse components [10]. ${}^{g}\mathbf{K}_n$ is the passage matrix from beam's local frame (n) to global reference frame (g), and

$$ u(\boldsymbol{\rho}, z) = u_0(z) \exp\left\{-j\frac{k}{2}\boldsymbol{\rho}^{\mathrm{T}}\mathbf{Q}(z)\boldsymbol{\rho} + j\phi(z)\right\}, \quad (3) $$

is the Gaussian scalar function [10, 11, 9] describing the transverse field distribution, where $\boldsymbol{\rho}$ is the transverse position vector, and z the longitudinal position, both written in the local reference frame (n) of the beam.

The couple of coefficients $\boldsymbol{\alpha}$ is computed during the expansion procedure using a point matching technique described in [**mypaper**, 10], and referred to as GBE. The set of beams is then launched through the quasi-optical system and a bouncing and tracing operation (GBT) is applied to find and track the reflected and refracted beams at each interface. The transverse coefficients $\boldsymbol{\alpha}_r$ and $\boldsymbol{\alpha}_t$ of, respectively, reflected and refracted beams, are computed using Fresnel formulas [12, 11].

A tangent frame to the surface, referred as (uv), is defined to account for the curvature of the surface intersecting the incident beam. The (uv) frame axes are $\hat{\boldsymbol{v}} \equiv \hat{\boldsymbol{y}}_i$ and $\hat{\boldsymbol{u}} = \hat{\boldsymbol{v}} \times \hat{\boldsymbol{n}}$. The computation of the curvature matrices ${}^{uv}\mathbf{Q}_r$ and ${}^{uv}\mathbf{Q}_t$ of the generated beams is performed in this frame, using a phase matching technique [11] and results in the following expressions :

$$ {}^{uv}\mathbf{Q}_r = {}^{uv}\mathbf{Q}_i - 2\,{}^{uv}\mathbf{C}\left(\hat{\boldsymbol{n}} \cdot \hat{\boldsymbol{z}}_i - \hat{\boldsymbol{n}} \cdot \hat{\boldsymbol{z}}_r\right) \quad (4a) $$

$$ {}^{uv}\mathbf{Q}_t = \frac{n_i}{n_t}\left\{ {}^{uv}\mathbf{Q}_i - {}^{uv}\mathbf{C}\left(\hat{\boldsymbol{n}} \cdot \hat{\boldsymbol{z}}_i - \frac{n_t}{n_i}\hat{\boldsymbol{n}} \cdot \hat{\boldsymbol{z}}_t\right)\right\} \quad (4b) $$

where ${}^{uv}\mathbf{C} \in \mathbf{R}^{2\times 2}$ is the surface curvature matrix at the intersection point. ${}^{uv}\mathbf{Q}_r$ and ${}^{uv}\mathbf{Q}_t$ are then expressed in the local frame of the reflected and refracted beams, respectively. In the studies presented in [11], both the Gouy phase η and the accumulated phase ϕ_{ac} are neglected during the phase matching. However, accounting for these phases is essential to prevent phase discontinuities. Furthermore, the amplitude of each beam is defined relative to the position of their respective beam waists. Due to the misalignment of these positions, an amplitude correction is also required. Consequently, a coupling term $a_0 \exp\{j\phi_0\}$ must be introduced to ensure accurate modelling,

$$ a_{0,g} = \frac{|u_i(\mathbf{0}, d_i)|}{u_{0,g}(\mathbf{0}, 0)}, \quad g \in \{r, t\}, \quad (5a) $$

$$ \phi_{0,g} = \angle u_i(\mathbf{0}, d_i) - \eta_g(0), \quad g \in \{r, t\}. \quad (5b) $$

where d_i represents the distance between the intersection point and the origin of the incident beam. The subscript i refers to the incident beam, while g is used to denote either the refracted beam (t) or the reflected beam (r).

B. S-parameter computation for a 2-port system

The electrical field at a point $\boldsymbol{r}$ (such as in the aperture of the receiving horn) is obtained using the recombination formula given by:

$$ {}^{g}\boldsymbol{E}({}^{g}\boldsymbol{r}) \approx \sum_{n=1}^{N} {}^{g}\mathbf{K}_n \, {}^{n}\boldsymbol{E}_{gb,n}({}^{n}\boldsymbol{r}). \quad (6) $$

Diagonal horns are used in the characterisation bench previously presented. The bench configuration is a two-port system as depicted in Fig. 2. The diagonal horns can be modelled by a square aperture rotated by $45°$ around the longitudinal axis z, in which lie two dominant modes: TE_{01} and TE_{10}. Assuming two identical horns, effects induced by the length of the horns can be ignored, as they will be removed by the calibration step. The received electrical field $\boldsymbol{E}$ at a horn aperture Ap is expressed as a combination of guided modes [13, p.120]. Considering only TE modes, this gives

$$ \boldsymbol{E} \approx c_{01}\boldsymbol{e}_{01} + c_{10}\boldsymbol{e}_{10} \quad (7) $$

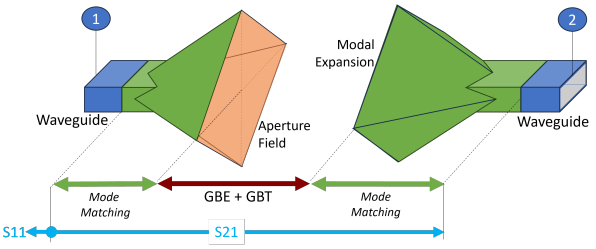

Fig. 2: A two-port system composed of two diagonal horns. The quasi-optical system, including the focusing lenses, is placed between the two horns.

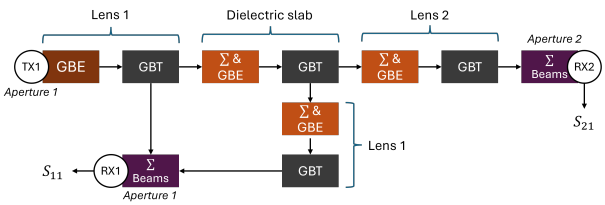

Fig. 3: Modelling pipeline, where Σ stands for beam summation, GBE for Gaussian Beam Expansion and GBT for Gaussian Beam Tracking.

where $\boldsymbol{e}_{01}$ is the field due to the TE_{01} mode and $\boldsymbol{e}_{10}$ the one for TE_{10}. The modal coefficients c_{01} and c_{10} are can be computed using the orthonormal properties of these modes [13]. This gives

$$c_k = \iint_{Ap} \boldsymbol{E} \times \boldsymbol{h}_k^* \cdot \hat{\boldsymbol{z}} dS \tag{8}$$

where $\boldsymbol{h}_k$ is magnetic field of the guided mode k.

Diagonal horn can be quickly simulated using mode matching techniques [13]. In order to do so, it could be assumed without loss of precision that the power is equally distributed between the TE_{01} and TE_{10} modes. However, in the actual bench, the excitation is a TE_{01} mode propagating in the feeding waveguide, which split into two modes of equal power once the waves travel in the horn's diagonal section. In order to estimate the transmission or reflection parameters, an averaging of c_{01} and c_{10} is calculated on the relevant aperture, rather than computing the coefficient of the fundamental mode propagating in the waveguide feeding this aperture. This avoid unnecessary complexity by assuming the horn length does not have significant effect, as previously discussed.

IV. Modelling of an Ideal Characterisation Bench with Calibration

The quasi-optical components of the characterisation bench previously presented are modelled using 3D models generated by computer-aided design tools. In order to exploit them, the free Gmsh software [14] for generating 3D meshes with support for pre- and post-processing is used. It can discretise surfaces and create geometric structures suitable for beam launching. Figure 3 shows the configuration of the bench modelling.

Using GBE and GBT, introduced in the previous section, we can decompose the electromagnetic field into elementary Gaussian beams and propagate these Gaussian beams through the optical system. The accuracy of the beam tracking decreases as propagating distance of the elementary beams increases. If the distance between two quasi-optical elements is large enough to avoid significant coupling, it becomes relevant to recombine and re-decompose the electromagnetic field just before the new element to be taken into account. Multi-path effects between the two elements are neglected, and only the reflection of the signal towards the lens is processed in a new beam launch. Several decomposition surfaces are then required.

A frequency sweep over the 220-330 GHz band is performed. Ports 1 and 2 of the system correspond to the aperture of the diagonal horns, where a modal analysis is performed as presented before. In order to model the calibration process, it is necessary to simulate each of its steps, each of which has a specific configuration as defined in **??**. An S2P file is generated for each step, to be used for extracting the MUT's S-parameters. As the system is passive, only the Port 1 → Port 2 direction is required here.

In addition, as the lenses are not moved in relation to their respective horns, the multiple reflection of the incident beam in these lenses will be identical, whether during calibration or measurement. These reflections should therefore be perfectly corrected during calibration. Note that this is no longer true if a lens shift or tilt exists between the calibration and measurement steps. The magnitude of the S-parameters obtained during calibration, depicted in Figure 4, shows the effect of the lens acting as a dielectric resonator due to the multiple reflections.

The system modelled and presented in Fig. 3 is passive. Therefore, as with the calibration, only the transmission direction from Port 1 to Port 2 is simulated, assuming that $S_{21,s} = S_{12,s}$.

The procedure developed in [6, 15] is used to apply the TRL calibration to the simulated S-parameters. Fig. 5 displays the extracted S-parameters, compared with the parameters calculated with the analytical model [6].

As can be seen in Fig. 5, there is no ripple on the reflection coefficient curve. The TRL correction effectively removes this effect in the case where no misalignment is present in the system.

Fig. 6 also shows good agreement between the measurements and the simulation. In the case of a system close to the ideal setup, placing the slab at the waist of the beam is almost equivalent to expose it to a plane wave incidence. The analytical model used to extract the permittivity of the dielectric slab, which assumes plane-

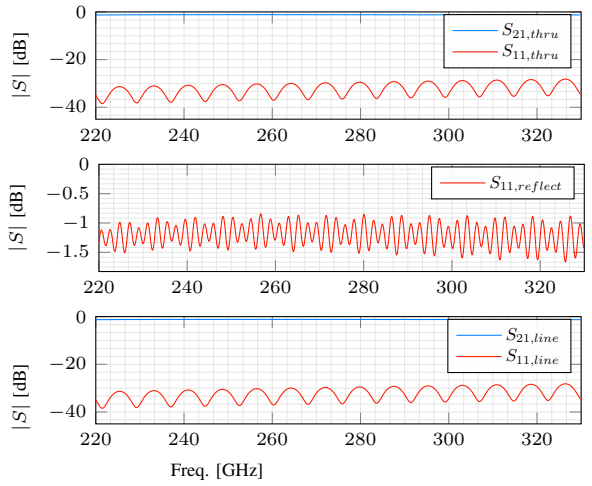

Fig. 4: Magnitude of transmission and reflection coefficients for the Port 1 $\rightarrow$ Port 2 direction, for the three calibration steps Thru-Reflect-Line. This shows the effect of the lens acting as a dielectric resonator.

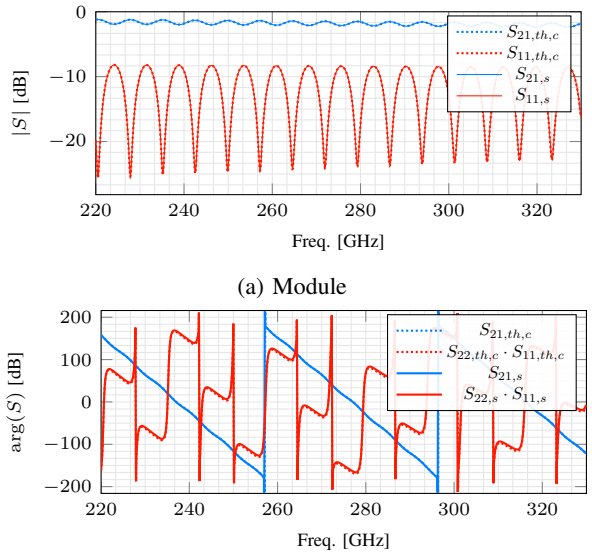

(a) Module

(b) Phase

Fig. 5: Simulated reflection and transmission parameters of a 12.825mm thick dielectric plate, compared with the analytical model, with $\epsilon_r = 2.5329 - 0.00667j$.

wave illumination, is therefore quite valid in this case.

V. Modelling of a Realistic Characterisation Bench

When setting up the test bench, positioning errors, such as small tilts or transverse offsets are unavoidable. Although these defects can be often negligible, they can nevertheless introduce disturbances into the measurements, particularly at very high frequency operation,

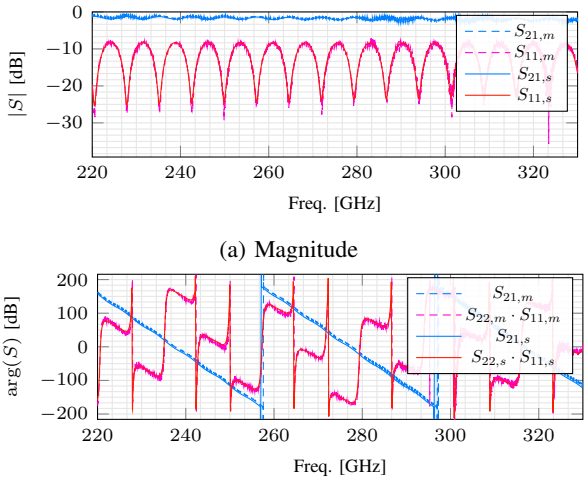

(a) Magnitude

(b) Phase

Fig. 6: Simulated reflection and transmission parameters of a 12.825mm thick dielectric slab, compared with the measurements, with $\epsilon_r = 2.5329 - 0.00667j$.

as in the J band. In this section, we study the impact of the defects, such the one presented in Table I, in a quasi-optical experimental setup on the accuracy of S-parameter measurements.

	Offsets [mm]			Tilts [°]	
	x	y	z	x	y
Lens 1	-3	2	2	1	2
Lens 2	1	-2	3	-1.2	1.5
Slab	0.96	-0.5	1.2	-0.2	0.9

TABLE I: Tilts and offsets applied to the lenses and slab.

Figure 7 shows that the extraction of the calibrated parameter S_{21} remains very close to the theoretical values, both in magnitude and phase, even in the presence of slight misalignments. This simulation, which reproduces a realistic experimental setup, highlights the robustness of the bench when combined with a TRL calibration. The small inclinations and offsets simulated have a minimal impact on the results, validating the calibration efficiency in compensating these imperfections existing in actual setup configurations.

VI. Conclusion

The modelling tool presented in this paper was employed to simulate a characterisation bench operating in the J-band (220-330 GHz). The results of this study demonstrate the tool's capability in predicting the overall behaviour and performance of the bench.

The developed simulator provides significant advantages, particularly in its potential to design optimised setups before they are physically implemented. By simulating the experimental bench configuration, one can

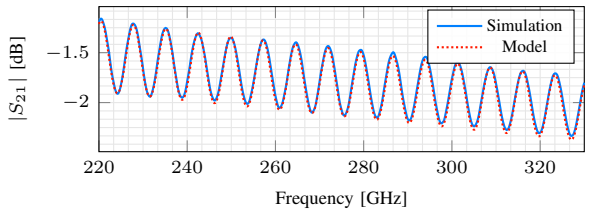

(a) Magnitude of S_{21} after calibration (blue). The dotted red curve corresponds to the magnitude value given by the analytical model with no offset.

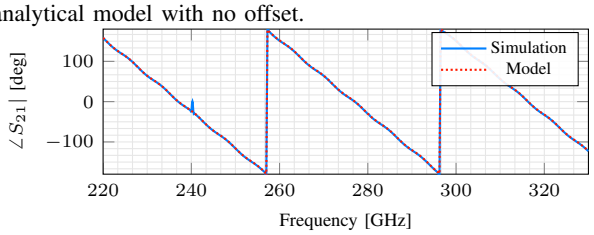

(b) Phase of S_{21} after calibration (blue). The dotted red curve corresponds to the phase value given by the analytical model with no offset.

Fig. 7: Simulated transmission parameter of a dielectric plate of $12.825\,\mathrm{mm}$ thickness, compared with the analytical model, with $\epsilon_r = 2.5329 - 0.00667j$, over the frequency range 220-330GHz. A combination of defects is applied on lenses and sample in order to reproduce a realistic measurement bench.

identify potential issues and makes necessary adjustments to enhance the system's performance without costly and time-consuming trial-and-error experiments. This foresight not only minimises the risk of design flaws but also reduces the resources required during the manufacturing and testing phases. As a result, the modelling tool proves to be a valuable asset in the design, optimisation, and improvement of quasi-optical systems and devices.

References

[1] Óscar García Pérez, F. Tercero, and Samuel Lopez Ruiz. *Free-space W-band setup for the electrical characterization of materials and mm-wave components*. Tech. rep. Observatorio de Yebes Guadalajara (Spain), June 2017.

[2] Elena Saenz, Luis Rolo, Kees Van't Klooster, Maurice Paquay, and Vladimir V. Parshin. "Accuracy assesment of material measurements with a quasi-optical free-space test bench". In: *6th European Conference on Antennas and Propagation (EuCAP)*. Mar. 2012, pp. 572–576. ISBN: 978-1-4577-0918-0. DOI: 10.1109/EuCAP.2012.6206324.

[3] Hong Eun Choi, Wonjin Choi, Evgenya I. Simakov, Muhammed Zuboraj, Bruce E. Carlsten, and EunMi Choi. "Error Tolerant Method of Dielectric Permittivity Determination Using a TE01 Mode in a Circular Waveguide at the W -Band". In: *IEEE Transactions on Microwave Theory and Techniques* 68.2 (2020), pp. 808–815. DOI: 10.1109/TMTT.2019.2951156.

[4] Nicolas Pantano, John Slabbekoorn, Fabrice Duval, and Eric Beyne. "Broadband permittivity characterization of polymers up to 110 GHz using co-planar waveguides". In: *2021 IEEE 71st Electronic Components and Technology Conference (ECTC)*. 2021, pp. 1252–1257. DOI: 10.1109/ECTC32696.2021.00203.

[5] Jonathan Hammler, Andrew Gallant, and Claudio Balocco. "Free-Space Permittivity Measurement at Terahertz Frequencies With a Vector Network Analyzer". In: *IEEE Transactions on Terahertz Science and Technology* 6 (Oct. 2016). DOI: 10.1109/TTHZ.2016.2609204.

[6] Daniel Bourreau and Alain Péden. "Solid and Non-Solid Dielectric Material Characterization for Millimeter and Sub-Millimeter Wave Applications". In: *2020 50th European Microwave Conference (EuMC)*. 2021, pp. 909–912. DOI: 10.23919/EuMC48046.2021.9338045.

[7] Gregory Gaudin, Daniel Bourreau, Clément Henry, and Alain Peden. "Modeling of Quasi-Optical Systems and Measurements with a Cobot in the J-Band". In: *18th European Conference on Antennas and Propagation (EuCAP2024)*. 2024 18th European Conference on Antennas and Propagation (EuCAP). Glasgow, United Kingdom: IEEE, Mar. 2024. DOI: 10.23919/EuCAP60739.2024.10501609. URL: https://hal.science/hal-04615494.

[8] Glenn F. Engen and Cletus A. Hoer. "Thru-Reflect-Line: An Improved Technique for Calibrating the Dual Six-Port Automatic Network Analyzer". In: *IEEE Transactions on Microwave Theory and Techniques* 27.12 (1979), pp. 987–993. DOI: 10.1109/TMTT.1979.1129778.

[9] Paul F. Goldsmith. "Gaussian Beam Propagation". In: *Quasioptical Systems: Gaussian Beam Quasioptical Propogation and Applications*. Wiley-

IEEE Press, 1998, pp. 9–38. ISBN: 978-0-470-54629-1. DOI: 10.1109/9780470546291.ch2.

[10] Alexandre Chabory, Jérôme Sokoloff, Sylvain Bolioli, and Paul François Combes. “Computation of electromagnetic scattering by multilayer dielectric objects using Gaussian beam based techniques”. In: *Comptes Rendus Physique* 6.6 (July 2005), pp. 654–662. ISSN: 16310705. DOI: 10.1016/j.crhy.2005.06.011.

[11] Evgenia Kochkina, Gudrun Wanner, Dennis Schmelzer, Michael Tröbs, and Gerhard Heinzel. “Modeling of the general astigmatic Gaussian beam and its propagation through 3D optical systems”. In: *Applied Optics* 52.24 (Aug. 2013), pp. 6030–6040. DOI: 10.1364/AO.52.006030.

[12] Arash Rohani, Amir Ahmad Shishegar, and S. Safavi-Naeini. “A fast Gaussian beam tracing method for reflection and refraction of general vectorial astigmatic Gaussian beams from general curved surfaces”. In: *Optics Communications* 232 (Mar. 2004), pp. 1–10. DOI: 10.1016/j.optcom.2003.11.044.

[13] Jorge Ruiz-Cruz, José Montejo-Garai, and Jesus Rebollar. “Computer Aided Design of Waveguide Devices by Mode-Matching Methods”. In: *Passive Microwave Components and Antennas*. Ed. by Vitaliy Zhurbenko. InTech, Apr. 2010. ISBN: 978-953-307-083-4. DOI: 10.5772/9403.

[14] Christophe Geuzaine and Jean-François Remacle. “Gmsh: A 3-D Finite Element Mesh Generator with built-in Pre- and Post-Processing Facilities”. In: *International Journal for Numerical Methods in Engineering* 79.11 (Sept. 2009), pp. 1309–1331. ISSN: 00295981. DOI: 10.1002/nme.2579.

[15] Daniel Bourreau, Alain Peden, and Sandrick Maguer. “A Quasi-Optical Free-Space Measurement Setup Without Time-Domain Gating for Material Characterization in the W-Band”. In: *Instrumentation and Measurement, IEEE Transactions on* 55 (Jan. 2007), pp. 2022–2028. DOI: 10.1109/TIM.2006.884283.